Dynamic Aggregation of Grid-tied Three-phase Inverters

Victor Purba, *Student Member*, *IEEE*, Brian B. Johnson, *Member*, *IEEE*
Saber Jafarpour, *Member*, *IEEE*, Francesco Bullo, *Fellow*, *IEEE*, and Sairaj V. Dhople, *Member*, *IEEE*

***Abstract*—The number of grid-tied inverters interfacing renewable resources, energy-storage devices, and flexible loads in distribution networks is steadily increasing. State-space models for inverters are nonlinear and high dimensional which renders the task of modeling large numbers at the edge of the grid to be a difficult undertaking. To address this issue, we develop a distribution-network-cognizant aggregation approach that describes the collective dynamics of grid-tied three-phase inverters. Inverters are clustered based on effective impedances to an infinite bus (modeling the transmission-distribution boundary) and for each cluster, an aggregate dynamical model is developed to preserve the structure and order of each individual inverter state-space model. The K-means algorithm is leveraged for clustering and a suitable linearization of the power-flow equations reduces computational burden involved in determining terminal voltages for the clusters. Numerical simulation results for the IEEE 37-bus feeder system demonstrate the accuracy and computational benefits of the proposed aggregation method.**

***Index Terms*—Model reduction, phase-locked loop, three-phase inverter, voltage-source inverter.**

I. Introduction

This paper outlines a model-aggregation procedure for grid-tied three-phase inverters with the goal of capturing the time evolution of real- and reactive-power injections at the distribution-network feeder head while acknowledging power flows between the inverters. We examine the AC-timescale dynamics of a three-phase voltage source inverter (VSI) with an output LCL filter, where the control architecture is composed of an inner current-control loop, an outer power-control loop, and a phase locked loop (PLL) for grid synchronization. The aggregation method is presented with a broad level of generality (with respect to inverter topology, controllers, and filters), but it is worth mentioning that the examined topology is prototypical and is recognizably popular in the literature [1]–[6]. In addition to the grid-tied inverters, our model for the distribution network includes impedance loads interconnected to the inverters through lines modeled with Π-equivalent circuits. Individually modeling the dynamics of *all* inverters, interconnecting lines, and loads to glean insights into the collective behavior of the distribution network—with particular emphasis on the active- and reactive-power injected into the feederhead—is computationally intractable. As a solution, we outline a reduced-order model for the distribution network, where inverters are clustered based on electrical distances from the feederhead and an aggregated model is derived for each cluster. The proposed models hold the potential to be useful in several application settings. Few that immediately spring to mind include: capturing the impact of fast variations in irradiance on the output power of PV systems, modeling the impact of wind gusts on the output power of wind energy conversion systems, and uncovering the impact of changing setpoints of large collections of inverters by aggregators (for frequency regulation or other grid services) on their collective outputs.

We explain the fundamental idea and the contributions of this work over our previous efforts with the aid of the illustrative network composed of 4 inverters in Fig. 1a and corresponding reduced-order aggregate models of varying complexity in Figs. 1b–1d. The individual inverter model has 15 states and the transmission-distribution interface is modeled as an infinite bus (marked g). We are interested in describing the dynamic evolution of the real- and reactive-power injections (p_g and q_g, respectively) into the grid bus. The simplest aggregate model is obtained by ignoring the

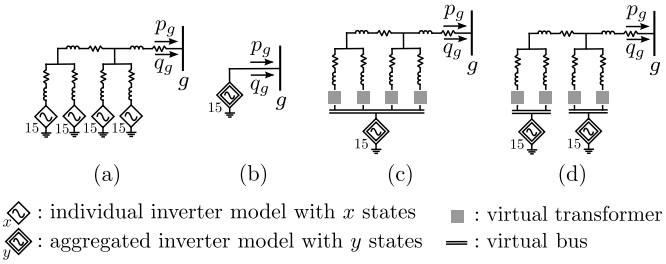

Fig. 1: (a) Network of 4 inverters. Dynamics of all inverters are captured by a $60(= 15 \times 4)$ order state-space model. (b) Reduced-order model of the system ignoring the network. Dynamics of all inverters are described by an aggregate 15 order model that has the same structure as any individual inverter. (c) Reduced-order model with all inverters aggregated into 1 group. As in (b), the aggregate model has 15 states. (d) Reduced-order model with inverters clustered into 2 groups. This model has $30(= 15 \times 2)$ states, but presents improved accuracy.

V. Purba and S. V. Dhople are with the Department of Electrical and Computer Engineering at the University of Minnesota (emails: {purba002,sdhople}@umn.edu); B. B. Johnson is with the Department of Electrical Engineering at the University of Washington (e-mail: brianbj@uw.edu); S. Jafarpour and F. Bullo are with the Center for Control, Dynamical Systems, and Computation at the University of California Santa-Barbara (emails: {saber.jafarpour, bullo}@engineering.ucsb.edu). Funding support from the U.S. Department of Energy Solar Energy Technologies Office under Contract No. DE-EE0000-1583, the National Science Foundation through grant 1453921, and the Washington Research Foundation is gratefully acknowledged.

electrical network (i.e., assuming all inverters are connected to the grid bus) and is illustrated in Fig. 1b. We showed in [7] that the aggregate model in this case has the same structure and model order as any inverter in the parallel system, albeit with suitably scaled model parameters. We extended the results in [7] to the case where the inverter power ratings are different and the inverters have different real- and reactive-power setpoints in [8]. A more accurate reduced-order model is shown in Fig. 1c and was examined in our earlier work [9] (and more recently in [10]). Here, we leveraged aggregation methods previously used for synchronous generators [11]–[13] to transfer all inverters to a single virtual bus, and then obtained the aggregate model as in Fig. 1b (following our work in [7], [8]). The virtual-transformer turns ratios are designed such that the voltages of the inverter-facing terminals are approximately the average of the voltages in the original network. To obtain an estimate of these voltages, we leverage linear approximations of the AC power flow equations [14]–[16]. In this work, we improve upon the network-agnostic aggregation in [7], [8] (Fig. 1b) and the single-virtual-bus aggregation in [9] (Fig. 1c) by introducing multiple virtual buses and clustering inverters to these buses according to their electrical distance from the grid bus (Fig. 1d). Subsequently, inverter models for each cluster are aggregated using the methods in [7], [8].

The intuition for having more than one virtual bus and to perform an electrical-distance-based clustering stems from the fact that the terminal voltage is an input to the inverter dynamical model, and the role of the PLL is to obtain the phase of the grid voltage. The model in Fig. 1b can only be expected to be accurate when interconnecting line parameters are such that they can be ignored, essentially implying that all inverters sense the same grid voltage. The model in Fig. 1c improves upon this with the average of the terminal voltages serving as a proxy to the actual inverter terminal voltages. Finally, the model in Fig. 1d is based on the underlying assumption that inverters that are electrically the same distance from the grid bus should be—in theory—dynamically coherent. This assumption is also leveraged in prior work on synchronous-generator coherency [11]–[13], [17] and network partitioning [18], [19], where, it is recognized that electrically close generators tend to swing together during disturbances. While the classic notion of coherency as it relates to machine angles does not perfectly translate to inverters [20], [21], we find that the electrical-distance-based clustering approach effectively identifies groups of inverters that have similar dynamic behavior during transients. Given its ease of implementation and scalability, we apply the K-means algorithm [22]–[24] to cluster inverters. With regard to determining the optimal number of clusters, we point to several numerical methods that have been proposed in the literature [25]–[30] to this end. For the present application, we find that the so-called silhouette analysis method [28]–[30] provides a good insight into the optimal number of clusters to be introduced.

From the perspective of model reduction, literature pertinent to our work is predominantly in the area of obtaining reduced-order models for individual inverters [31]–[33]. Our work differs by providing reduced-order models for collections of inverters. Also related are recent efforts that have sought to extend coherency-based clustering and collective aggregation to droop-controlled islanded inverters [34] and parallel-connected virtual-synchronous-generator-controlled multilevel converters [35]. However, the application setting in these works is that of grid-forming inverters controlled to emulate synchronous machines, and therefore, classical results from clustering synchronous machine models can be applied straightforwardly. The aggregation method outlined in this work can be applied to grid-forming inverters if an aggregated model for the elemental parallel connection is known. Such models have indeed been identified in the literature. For instance, [36] and [37] outline aggregate models for parallel-connected droop-controlled and virtual-oscillator-controlled inverters, respectively. For complex networks with heterogeneous inverter types, aggregation based on inverter control method and type (grid-forming, grid-following) as developed in [10] *in addition to* electrical distances would conceivably be necessary.

Before proceeding to technical details, we summarize all the key contributions of the paper. The main contribution of this work is the development of an approach to cluster inverters installed in a distribution network based on their electrical distances to the feederhead and a strategy to determine the optimal number of required clusters in a given distribution network. The proposed method is presented in the context of a very widely used inverter control architecture, and it applies to inverters with different power ratings and setpoints. As a concrete outcome, we deliver a compact state-space model representation for the distribution network that strikes the right balance between computational cost and modeling details.

The remainder of this paper is organized as follows. In Section II, we introduce the three-phase grid-connected inverter model and briefly review the aggregation results for parallel-connected inverters. In Section III, we describe the distribution feeder model. In Section IV, we outline the network-cognizant aggregation approach. We validate the proposed approach with exhaustive numerical simulations for an illustrative feeder network in Section V. Finally, concluding remarks and directions for future work are given in Section VI.

II. Inverter Model and Parallel Aggregation

This section briefly overviews the model of a single inverter, and the aggregate model for a parallel collection.

A. Inverter Model

We place the following discussion in context of the inverter model sketched in Fig. 2a. Key elements here are reference

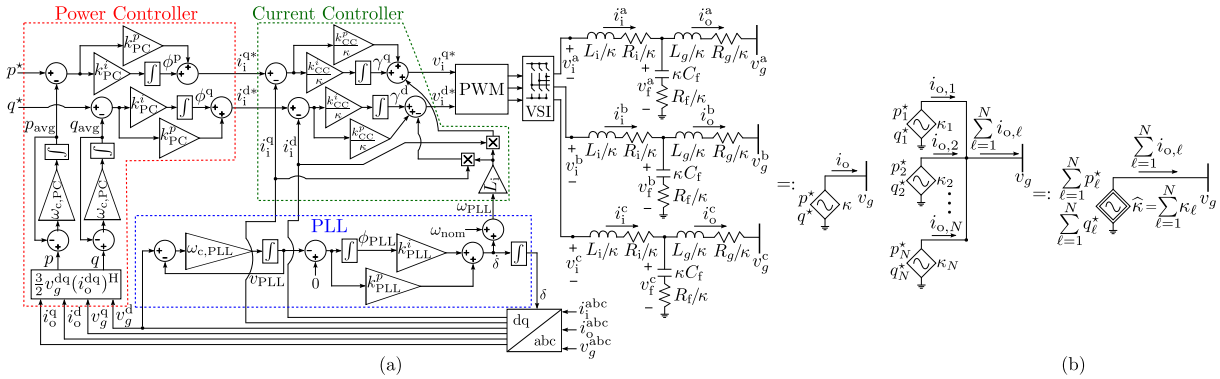

Fig. 2: (a) Feed-back control loops and output filter of the grid-tied three-phase inverter, and adopted shorthand depicting: i) power rating, with the aid of the power-scaling parameter, κ (see (2)), ii) real-power setpoint, $p^\star$, and iii) reactive-power setpoint, $q^\star$. (b) Parallel connection of N inverters, and the adopted shorthand representation of the reduced-order model. The reduced-order model has the same form as (a) with equivalent power-scaling parameter $\widehat{\kappa} = \sum_{\ell=1}^{N} \kappa_\ell$, real-power setpoint, $\sum_{\ell=1}^{N} p_\ell^\star$, and reactive-power setpoint, $\sum_{\ell=1}^{N} q_\ell^\star$.

frame transformations used to facilitate control, internal controller and filter dynamics, and power-scaling parameters that capture the different power ratings for the inverters.

1) Reference-frame transformations: Three-phase signals $x^{\mathrm{abc}} = [x^{\mathrm{a}}, x^{\mathrm{b}}, x^{\mathrm{c}}]^{\mathrm{T}}$ are transformed to equivalent DC signals $(x^{\mathrm{d}}, x^{\mathrm{q}})$ using Park's transformation implemented with the PLL angle, δ.[1] The abc-dq block in Fig. 2a captures the transformation. In a system of inverters, the controller for each inverter operates on signals in its own dq reference frame. For analytical convenience, inverter outputs and network variables should be represented in the same reference frame. To do so, it is common practice to rely on a global DQ frame with phase denoted by δ_g and frequency ω_g. Given variables in the local dq frame, x^{d} and x^{q}, the corresponding variables in the global reference frame are denoted by x^{D} and x^{Q}, and they are obtained through:

$$\begin{bmatrix} x^{\mathrm{D}} \\ x^{\mathrm{Q}} \end{bmatrix} = \begin{bmatrix} \cos(\delta_g - \delta) & \sin(\delta_g - \delta) \\ -\sin(\delta_g - \delta) & \cos(\delta_g - \delta) \end{bmatrix} \begin{bmatrix} x^{\mathrm{d}} \\ x^{\mathrm{q}} \end{bmatrix}. \tag{1}$$

For subsequent developments, we define $x^{\mathrm{DQ}} := x^{\mathrm{D}} + jx^{\mathrm{Q}}$ and $x^{\mathrm{dq}} := x^{\mathrm{d}} + jx^{\mathrm{q}}$.

2) State-space model for the inverter dynamics: A block diagram of the inverter control architecture is illustrated in Fig. 2a. To capture inverters with different power ratings, we define the *power-scaling parameter*, κ, as follows [7]:

$$\kappa = p_{\mathrm{rated}}/p_{\mathrm{base}}, \tag{2}$$

with p_{rated} and p_{base} denoting the rated power of the inverter and the system-wide base value, respectively. We assume a voltage source inverter (VSI) and an output LCL filter with inverter-side inductance, L_{i}, grid-side inductance, L_g, and filter capacitance, C_{f}. The control architecture consists of an inner-loop current controller, an outer-loop power controller, and a phase-locked loop (PLL). The power controller (PC) consists of two low pass filters and two PI controllers. The reference inputs to the controller are the real- and reactive-power setpoints (denoted by $p^\star$ and $q^\star$, respectively), its outputs are the references for the current controller. The current controller (CC) consists of two PI controllers and feedforward terms, with outputs to be the reference for the terminal voltage v_{i}. The PLL consists of a low pass filter and a PI controller. It synchronizes with the grid by modulating the angle δ such that $v_g^{\mathrm{d}} \to 0$. Inverters with power rating κp_{base} have parameters $L_{\mathrm{i}}, R_{\mathrm{i}}, C_{\mathrm{f}}, R_{\mathrm{f}}, L_g, R_g, k_{\mathrm{CC}}^p, k_{\mathrm{CC}}^i$ scaled as $\kappa^{-1}L_{\mathrm{i}}, \kappa^{-1}R_{\mathrm{i}}, \kappa C_{\mathrm{f}}, \kappa^{-1}R_{\mathrm{f}}, \kappa^{-1}L_g, \kappa^{-1}r_g, \kappa^{-1}k_{\mathrm{CC}}^p, \kappa^{-1}k_{\mathrm{CC}}^i$. This assumption is backed by several engineering rules of thumb. For instance, it ensures the voltage drop across the LCL filter and the closed-loop system response is identical across power levels. See [7] for more details.

The inverter dynamics discussed above can be compactly described by the following 15th-order model [7]:

$$\dot{x} = Ax + Bu_{\mathrm{s}} + g(x, u_{\mathrm{v}}), \quad y = i_{\mathrm{o}}^{\mathrm{DQ}}, \tag{3}$$

with states and inputs:

$$\begin{aligned} x = [&i_{\mathrm{i}}^{\mathrm{d}}, i_{\mathrm{i}}^{\mathrm{q}}, i_{\mathrm{o}}^{\mathrm{d}}, i_{\mathrm{o}}^{\mathrm{q}}, v_{\mathrm{f}}^{\mathrm{d}}, v_{\mathrm{f}}^{\mathrm{q}}, \\ &\gamma^{\mathrm{d}}, \gamma^{\mathrm{q}}, p_{\mathrm{avg}}, q_{\mathrm{avg}}, \phi^{\mathrm{p}}, \phi^{\mathrm{q}}, v_{\mathrm{PLL}}, \phi_{\mathrm{PPL}}, \delta]^{\mathrm{T}}, \end{aligned} \tag{4}$$

$$u_{\mathrm{s}} = [p^\star, q^\star]^{\mathrm{T}}, \quad u_{\mathrm{v}} = v_g^{\mathrm{abc}} := [v_g^{\mathrm{a}}, v_g^{\mathrm{b}}, v_g^{\mathrm{c}}]^{\mathrm{T}}. \tag{5}$$

In (4), $i_{\mathrm{i}}^{\mathrm{d}}$, $i_{\mathrm{i}}^{\mathrm{q}}$, $i_{\mathrm{o}}^{\mathrm{d}}$, $i_{\mathrm{o}}^{\mathrm{q}}$, $v_{\mathrm{f}}^{\mathrm{d}}$, and $v_{\mathrm{f}}^{\mathrm{q}}$ are native to the LCL filter (see Fig. 2a); γ^{d} and γ^{q} are states that capture the dynamics of the PI loop in the current controller; p_{avg}, q_{avg}, ϕ^{p}, and ϕ^{q} are states that capture the dynamics of averaging and the PI loop in the power controller; and v_{PLL}, ϕ_{PPL}, and δ are states that capture the dynamics of the low-pass filter and PI loop in the PLL. Input u_{s} captures the real- and reactive-power setpoints, and input u_{v} is the voltage sensed at the inverter terminals. The output of the state-space model, $y =$

[1] *Notation:* The matrix transpose is denoted by $(\cdot)^{\mathrm{T}}$. The Moore-Penrose pseudo inverse of a matrix B is denoted by $B^\dagger$. A diagonal matrix formed with the entries of vector x is denoted by $\mathrm{diag}(x)$; $\mathrm{bdiag}(A_1, \ldots, A_N)$ denotes a block diagonal matrix of $A_1, \ldots, A_N$. The entrywise natural logarithm and the smallest entry of vector x are denoted by $\log(x)$ and $\min(x)$, respectively; 1_N and 0_N denote N-dimension vectors of all one and all zero entries, respectively; I_N and $0_{M\times N}$ denote the $N \times N$ identity matrix and an $M \times N$ matrix of all zeros, respectively. Furthermore, $j = \sqrt{-1}$; the magnitude, angle, real and imaginary components of a complex variable x are denoted by $|x|$, $\angle x$, $\mathrm{Re}\{x\}$, and $\mathrm{Im}\{x\}$, respectively, and the matrix conjugate transpose is denoted by $(\cdot)^{\mathrm{H}}$. The cardinality of set $\mathcal{A}$ is denoted by $|\mathcal{A}|$. The maximum of two scalars, a and b, is denoted by $\max(a, b)$.

$i_{\rm o}^{\rm DQ} \in \mathbb{C}$ is the L_g-branch current represented in the global DQ reference frame (see Fig. 2a). Due to space constraints, we refrain from spelling out entries of A, B, and $g(\cdot,\cdot)$. Interested readers are referred to [7] for a detailed description of the inverter filter and controller dynamics.

B. Reduced-order Model of Parallel-connected Inverters

Consider a collection of N inverters, all with the dynamical model (3) connected in parallel to the grid bus. We capture the following types of heterogeneity in inverters:

1) The inverters have different power ratings. The power scaling parameter of the ℓ inverter is denoted by κ_ℓ.
2) The inverters have different reference-power setpoints. The real- and reactive-power setpoints for inverter ℓ are denoted by $p_\ell^\star$ and $q_\ell^\star$, respectively.

We have shown in [8] that the dynamics of this system of inverters can be described by a model with the same structure and order as any individual inverter (see Fig. 2a). (We note that the results in [8] are for single-phase inverters; the extension to the three-phase setting is straightforward.) The aggregated inverter dynamics can be compactly expressed with the following 15th-order state-space model:

$$\dot{\widehat{x}} = \widehat{A}\widehat{x} + \widehat{B}\widehat{u}_{\rm s} + \widehat{g}(\widehat{x},\widehat{u}_{\rm v}), \quad \widehat{y} = \widehat{i}_{\rm o}^{\rm DQ}, \tag{6}$$

with states and inputs:

$$\begin{aligned}\widehat{x} &= [\widehat{i}_{\rm i}^{\rm d}, \widehat{i}_{\rm i}^{\rm q}, \widehat{i}_{\rm o}^{\rm d}, \widehat{i}_{\rm o}^{\rm q}, \widehat{v}_{\rm f}^{\rm d}, \widehat{v}_{\rm f}^{\rm q},\\ &\widehat{\gamma}^{\rm d}, \widehat{\gamma}^{\rm q}, \widehat{p}_{\rm avg}, \widehat{q}_{\rm avg}, \widehat{\phi}^{\rm p}, \widehat{\phi}^{\rm q}, \widehat{v}_{\rm PLL}, \widehat{\phi}_{\rm PPL}, \widehat{\delta}]^{\rm T}, \end{aligned}\tag{7}$$

$$\widehat{u}_{\rm s} = \sum_{\ell=1}^{N}[p_\ell^\star, q_\ell^\star]^{\rm T}, \quad \widehat{u}_{\rm v} = v_g^{\rm abc} = [v_g^{\rm a}, v_g^{\rm b}, v_g^{\rm c}]^{\rm T}. \tag{8}$$

Input $\widehat{u}_{\rm s}$ captures the net real- and reactive-power setpoints of the inverters in the system, and input $\widehat{u}_{\rm v}$ is the voltage sensed at the inverter terminals, which in this case, is the grid voltage. The output of the state-space model, $\widehat{y} = \widehat{i}_{\rm o}^{\rm DQ} \in \mathbb{C}$ is the output current of the collection of inverters in the global DQ reference frame. Matrices $\widehat{A} \in \mathbb{R}^{15\times 15}$, $\widehat{B} \in \mathbb{R}^{15\times 2}$, and function $\widehat{g} : \mathbb{R}^{15} \times \mathbb{R}^3 \to \mathbb{R}^{15}$ have the same dimension and structure as A, B, and g for the individual inverter model. Their entries are obtained by replacing the individual inverter model parameters $L_{\rm i}, R_{\rm i}, C_{\rm f}, R_{\rm f}, L_g, R_g, k_{\rm CC}^p, k_{\rm CC}^i$ with $\widehat{\kappa}^{-1}L_{\rm i}, \widehat{\kappa}^{-1}R_{\rm i}, \widehat{\kappa}C_{\rm f}, \widehat{\kappa}^{-1}R_{\rm f}, \widehat{\kappa}^{-1}L_g, \widehat{\kappa}^{-1}r_g, \widehat{\kappa}^{-1}k_{\rm CC}^p, \widehat{\kappa}^{-1}k_{\rm CC}^i$, where $\widehat{\kappa} := \sum_{\ell=1}^N \kappa_\ell$ denotes the *equivalent power-scaling parameter*. The states of the aggregated inverter (7) relate to the individual inverter (4) as follows $\forall t \geq t_0$ [8]:

$$\begin{aligned}&[\widehat{i}_{\rm i}^{\rm d}, \widehat{i}_{\rm i}^{\rm q}, \widehat{i}_{\rm o}^{\rm d}, \widehat{i}_{\rm o}^{\rm q}, \widehat{\gamma}^{\rm d}, \widehat{\gamma}^{\rm q}, \widehat{p}_{\rm avg}, \widehat{q}_{\rm avg}, \widehat{\phi}^{\rm p}, \widehat{\phi}^{\rm q}]^{\rm T} =\\ &\sum_{\ell=1}^{N}[i_{{\rm i},\ell}^{\rm d}, i_{{\rm i},\ell}^{\rm q}, i_{{\rm o},\ell}^{\rm d}, i_{{\rm o},\ell}^{\rm q}, \gamma_\ell^{\rm d}, \gamma_\ell^{\rm q}, p_{{\rm avg},\ell}, q_{{\rm avg},\ell}, \phi_\ell^{\rm p}, \phi_\ell^{\rm q}]^{\rm T},\\ &[\widehat{v}_{\rm f}^{\rm d}, \widehat{v}_{\rm f}^{\rm q}]^{\rm T} = \frac{1}{N}\sum_{\ell=1}^{N}[v_{{\rm f},\ell}^{\rm d}, v_{{\rm f},\ell}^{\rm q}]^{\rm T},\\ &[\widehat{v}_{\rm PLL}, \widehat{\phi}_{\rm PPL}, \widehat{\delta}]^{\rm T} = [v_{{\rm PLL},\ell}, \phi_{{\rm PPL},\ell}, \delta_\ell]^{\rm T}, \forall \ell.\end{aligned}$$

III. Network Description and Dynamics

In this section, we describe the distribution-network topology and outline its dynamical model.

A. Distribution-network Topology and Constitution

We study the networked dynamics of inverters connected in a balanced three-phase electrical distribution network with the Π-model adopted for branches in the network [38]. Figure 3a illustrates the system: each inverter is pictorially represented with the shorthand established in Fig. 2a. The slack bus (representing the secondary of the step-down transformer that connects the distribution network to the bulk system) is denoted by g. The nodes of the electrical network and the grid are collected in the set $\mathcal{N} \cup \{g\}$, inverter buses are denoted by $\mathcal{I} \subseteq \mathcal{N}$, and $\mathcal{Z} = \mathcal{N} \setminus \mathcal{I}$ collects the set of buses with zero current injections. Branches are collected in the set $\mathcal{E} \subseteq \mathcal{N} \cup \{g\} \times \mathcal{N} \cup \{g\}$. The edge-incidence matrix of the network, $E \in \mathbb{R}^{(|\mathcal{N}|+1)\times|\mathcal{E}|}$, has entries

$$[E]_{k\ell} := \begin{cases} 1, & \text{if } k \text{ is the source of } \ell\text{-th line},\\ -1, & \text{if } k \text{ is the sink of } \ell\text{-th line},\\ 0, & \text{otherwise.}\end{cases} \tag{9}$$

Furthermore, we will find it useful to define $F := [{\rm I}_{|\mathcal{I}|}, 0_{(|\mathcal{N}|+1)\times|\mathcal{I}|}^{\rm T}]^{\rm T}$.

Let $R_\mathcal{E} \in \mathbb{R}^{|\mathcal{E}|}$, $L_\mathcal{E} \in \mathbb{R}^{|\mathcal{E}|}$, and $C_\mathcal{E} \in \mathbb{R}^{|\mathcal{N}|}$ denote the vectors that collect the line resistance, line inductance, and shunt capacitance, respectively. The network admittance matrix, $Y \in \mathbb{C}^{(|\mathcal{N}|+1)\times(|\mathcal{N}|+1)}$, maps the nodal voltages to the current injections, and it is given by:

$$Y := E{\rm diag}(R_\mathcal{E} + j\omega_g L_\mathcal{E})^{-1}E^{\rm T} + j\omega_g {\rm diag}([C_\mathcal{E}^{\rm T}, 0]^{\rm T}). \tag{10}$$

Nodal voltages and current injections in the DQ reference frame are $v^{\rm DQ} := [(v_\mathcal{N}^{\rm DQ})^{\rm T}, v_g^{\rm DQ}]^{\rm T}$ and $i^{\rm DQ} := [(i_\mathcal{N}^{\rm DQ}, -i_g^{\rm DQ})^{\rm T}]^{\rm T}$ (the negative sign that precedes $i_g^{\rm DQ}$ is in acknowledgment of its assumed direction as shown in Fig. 3a). It follows that $i_\mathcal{N}^{\rm DQ} = [(i_\mathcal{I}^{\rm DQ})^{\rm T}, 0_{|\mathcal{Z}|}^{\rm T}]^{\rm T}$ and $v_\mathcal{N}^{\rm DQ} = [(v_\mathcal{I}^{\rm DQ})^{\rm T}, (v_\mathcal{Z}^{\rm DQ})^{\rm T}]^{\rm T}$. Finally, $i_\mathcal{E}^{\rm DQ} \in \mathbb{C}^{|\mathcal{E}|}$ collects the directed currents of the lines, and $i_{{\rm o}\mathcal{I}}^{\rm DQ} \in \mathbb{C}^{|\mathcal{I}|}$ is the vector that collects output currents of the inverters on the L_g branches. While $i_{{\rm o}\mathcal{I}}^{\rm DQ} = i_\mathcal{I}^{\rm DQ}$ in the original network, we will note that $i_{{\rm o}\mathcal{I}}^{\rm DQ} \neq i_\mathcal{I}^{\rm DQ}$ in the virtual circuit with virtual transformers (see Fig. 3b). We introduce no additional notation to distinguish between time- and phasor-domain representations of variables. Differences are expected to be contextually clear.

B. DQ-frame Network Dynamics in the Time Domain

In their original form, and without any model reduction, the dynamics of the distribution feeder include those arising from the interconnecting distribution lines and inverters. With a slight abuse of notation compared to (3), the dynamics of all inverters in the system are given by

$$\begin{aligned}\dot{x} &= {\rm bdiag}(A_1, \ldots, A_{|\mathcal{I}|})x + [(B_1 u_{{\rm s},1})^{\rm T}, \ldots, (B_{|\mathcal{I}|}u_{{\rm s},|\mathcal{I}|})^{\rm T}]^{\rm T}\\ &+ g'(x, u_{\rm v}), \quad y = i_{{\rm o}\mathcal{I}}^{\rm DQ},\end{aligned}\tag{11}$$

where $x := [x_1^{\mathrm{T}}, \ldots, x_{|\mathcal{I}|}^{\mathrm{T}}]^{\mathrm{T}} \in \mathbb{R}^{15|\mathcal{I}|}$ collects the states corresponding to all inverters in the system (each $x_\ell \in \mathbb{R}^{15}$ has entries shown in (4)), $g' : \mathbb{R}^{15|\mathcal{I}|} \times \mathbb{R}^{3\times|\mathcal{I}|} \to \mathbb{R}^{15|\mathcal{I}|}$ is:

$$g'(x, u_{\mathrm{v}}) = [g_1(x_1, v_{\mathrm{v},1})^{\mathrm{T}}, \ldots, g_{|\mathcal{I}|}(x_{|\mathcal{I}|}, v_{\mathrm{v},|\mathcal{I}|})^{\mathrm{T}}]^{\mathrm{T}},$$

with A_ℓ, B_ℓ, and g_ℓ above defined in the state-space model of an individual inverter as in (3). Finally, $u_{\mathrm{s},\ell} = [p_\ell^\star, q_\ell^\star]^{\mathrm{T}}$ captures the real- and reactive-power setpoints of the ℓ-th inverter, and $u_{\mathrm{v}} = v_{\mathcal{I}}^{\mathrm{abc}}$ captures inverter voltages in the abc reference frame. The line-current and bus-voltage dynamics in the network in the DQ-frame are given by

$$\begin{aligned} \mathrm{diag}(L_{\mathcal{E}})\dot{i}_{\mathcal{E}}^{\mathrm{DQ}} &= -\mathrm{diag}(R_{\mathcal{E}} + j\omega_g L_{\mathcal{E}})i_{\mathcal{E}}^{\mathrm{DQ}} + E^{\mathrm{T}} v^{\mathrm{DQ}}, \quad (12)\\ \mathrm{diag}(C_{\mathcal{E}})\dot{v}_{\mathcal{N}}^{\mathrm{DQ}} &= -j\omega_g \mathrm{diag}(C_{\mathcal{E}})v_{\mathcal{N}}^{\mathrm{DQ}} + F_{\mathcal{N}} i_{\mathrm{o}\mathcal{I}}^{\mathrm{DQ}} - E_{\mathcal{N}} i_{\mathcal{E}}^{\mathrm{DQ}}, \end{aligned}$$

where, recall that E is the network edge-incidence matrix (9), and matrices $F_{\mathcal{N}} \in \mathbb{R}^{|\mathcal{N}|\times|\mathcal{I}|}$ and $E_{\mathcal{N}} \in \mathbb{R}^{|\mathcal{N}|\times|\mathcal{E}|}$ are obtained from F and E by discarding the row that corresponds to the grid bus. The current injected into the grid, i_g, in Fig. 3a, is given by $i_g^{\mathrm{DQ}} = -E_g i_{\mathcal{E}}^{\mathrm{DQ}}$, where E_g denotes the row in E corresponding to the grid bus. The real- and reactive-power injections into the grid bus are given by

$$p_g = \frac{3}{2}(v_g^{\mathrm{D}}\, i_g^{\mathrm{D}} + v_g^{\mathrm{Q}}\, i_g^{\mathrm{Q}}), \quad q_g = \frac{3}{2}(v_g^{\mathrm{Q}}\, i_g^{\mathrm{D}} - v_g^{\mathrm{D}}\, i_g^{\mathrm{Q}}). \quad (13)$$

With all dynamics explicitly modeled in (11), (12), the order of the dynamical model one has to simulate to obtain the time-domain evolution of p_g and q_g is $2(|\mathcal{E}| + |\mathcal{N}|) + 15|\mathcal{I}|$.

IV. Network-cognizant Aggregate Model

In this section, we present the details of the clustering approach and the aggregate dynamical model. The aggregation strategy applies to any connected network topology (meshed, radial) with arbitrary line impedance values.

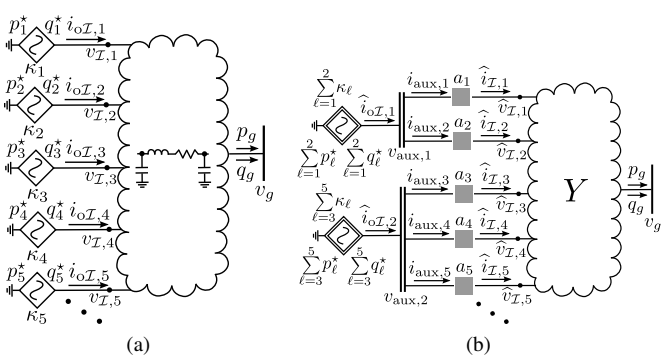

Fig. 3: Illustrating adopted notation and aggregate model: (a) Network of $|\mathcal{I}|$ inverters with different power ratings and reference-power setpoints (five of which are explicitly illustrated) with Π-equivalent circuits adopted to model interconnecting lines. (b) Reduced-order model of the system with the inverters aggregated into clusters (two of which are explicitly illustrated) determined based on electrical distances from bus g that denotes the transmission-distribution interface.

A. Virtual Network with Aggregated Inverters

To describe the circuit equations that underlie the reduced-order model, consider the network sketched in Fig. 3b, where inverters have been clustered (and subsequently aggregated) based on the electrical distances between their terminals and the grid bus in the originating network sketched in Fig. 3a. In subsequent developments, this network with clustered and aggregated inverters is referred to as the *virtual network*. Let $\widehat{i}_{\mathrm{o}\mathcal{I}}^{\mathrm{DQ}} \in \mathbb{C}^{|\mathcal{C}|}$ denote the vector that collects the output current of the aggregated inverters, $i_{\mathrm{aux}}^{\mathrm{DQ}} \in \mathbb{C}^{|\mathcal{I}|}$ captures the currents from the virtual buses into the primary side of the transformers, and $\widehat{i}_{\mathcal{I}}^{\mathrm{DQ}} \in \mathbb{C}^{|\mathcal{I}|}$ captures the currents from the secondary-side of the transformers into the electrical network. Similarly, $\widehat{v}_{\mathcal{I}}^{\mathrm{DQ}} \in \mathbb{C}^{|\mathcal{I}|}$ captures the voltages on the secondary-side of the transformers, and $v_{\mathrm{aux}}^{\mathrm{DQ}} \in \mathbb{C}^{|\mathcal{C}|}$ denotes the voltages on the primary side. See Fig. 3b for an illustration of these variables. Denote $\mathcal{I}_c$ as the index set of inverter buses that belong to the c-th cluster. For subsequent developments, we will find matrix $\Phi \in \mathbb{R}^{|\mathcal{I}|\times|\mathcal{C}|}$ with entries:

$$[\Phi]_{kc} := \begin{cases} 1, & \text{if } k \in \mathcal{I}_c, \\ 0, & \text{otherwise}, \end{cases}$$

useful in identifying the clusters that inverters belong to.

1) Clustering of inverters: We use the effective impedance as a measure of the electrical distance. The effective impedance between the grid bus, g, and the ℓ-th inverter bus, denoted by $z_{g\ell}^{\mathrm{eff}} \in \mathbb{C}$, is defined as the potential difference between these two buses when a unit current is injected in bus g and extracted from bus ℓ. It can be computed as [39]:

$$z_{g\ell}^{\mathrm{eff}} = (e_g - e_\ell)^{\mathrm{T}} v = (e_g - e_\ell)^{\mathrm{T}} Y^\dagger (e_g - e_\ell), \quad (14)$$

where $Y^\dagger$ is the pseudoinverse of the network admittance matrix, $e_g \in \mathbb{R}^{|\mathcal{N}|+1}$ and $e_\ell \in \mathbb{R}^{|\mathcal{N}|+1}$ denote the canonical vectors of all zeros except with entry one at the position of index g (i.e., the grid bus) and index ℓ (capturing the inverter at bus $\ell \in \mathcal{I}$), respectively. Let $z^{\mathrm{eff}} \in \mathbb{R}^{|\mathcal{I}|}$ denote the vector that collects all the magnitudes of effective impedances between the grid bus and inverter buses. With this measure of electrical distance, we utilize the K-means algorithm to group the inverters into $|\mathcal{C}|$ clusters [23], [24]. We apply the algorithm to a pre-processed version of z^{eff}, denoted by $z_{\mathrm{scaled}}^{\mathrm{eff}} \in \mathbb{R}_{\geq 0}^{|\mathcal{I}|}$, and defined by:

$$z_{\mathrm{scaled}}^{\mathrm{eff}} := \log\left(z^{\mathrm{eff}} / \min(z^{\mathrm{eff}})\right). \quad (15)$$

We scale z^{eff} by the inverse of its smallest entry so that its logarithm is nonnegative. Clustering based on entries of $z_{\mathrm{scaled}}^{\mathrm{eff}}$ is noted empirically to yield better results, i.e., with a higher probability, inverters farther away from the grid bus are clustered together.

2) Determining the Optimal Number of Clusters: One method to measure the quality of clustering is silhouette analysis [28]–[30]. For a point $a \in \mathcal{C}_\ell$, let $d(a)$ denote the average of the distance between point a and other points inside cluster $\mathcal{C}_\ell$, $\widetilde{d}_k(a, \mathcal{C}_k)$ denote the average of the distance between point a and all other points in cluster $\mathcal{C}_k$, where

$k \neq \ell$, and the minimum of all $\widetilde{d}_k(a, \mathcal{C}_k)$ values is denoted by $\widetilde{d}(a)$. The silhouette value of point a, denoted by $s(a)$, is given by: [30]

$$s(a) = \frac{\widetilde{d}(a) - d(a)}{\max(d(a), \widetilde{d}(a))}. \tag{16}$$

Note that the range of $s(a)$ is between -1 and 1. Observing (16), $s(a)$ has a negative value if $\widetilde{d}(a) < d(a)$, and a value close to 1 if $\widetilde{d}(a) \gg d(a)$. With K-means, the sum of within-cluster distances decreases as the number of clusters increases, therefore, the average silhouette value of all the points tends to approach unity. Without loss of generality, we choose the number of clusters with average silhouette value around 0.8 as the optimal number of clusters for simulations that follow. The silhouette analysis method outlined above is one of many [25]–[30] that have been proposed in the literature for determining the optimal number of clusters. Empirically, we observe that this yields good results for the considered application.

3) Engineering the virtual network: The formulation of the virtual network (Fig. 3b) hinges on the choice of the virtual-transformer turns ratios. One option is to pick the nominal virtual-bus voltages, $\overline{v}_{\rm aux}^{\rm DQ} \in \mathbb{C}^{|\mathcal{C}|}$ to be the weighted average of the inverter-terminal voltages:

$$\overline{v}_{\rm aux}^{\rm DQ} = {\rm diag}(({\rm diag}(K)\Phi)^{\rm T} 1_{|\mathcal{I}|})^{-1} ({\rm diag}(K)\Phi)^{\rm T} v_{\mathcal{I}}^{\rm DQ}, \tag{17}$$

where $K := [\kappa_1, \ldots, \kappa_{|\mathcal{I}|}]^{\rm T}$. Above, $v_{\mathcal{I}}^{\rm DQ}$ collects the inverter terminal voltages *in the original network* (Fig. 3a). This is a key point and deserves emphasis. The choice in (17) establishes the link between the original and virtual networks. Simulating the dynamics of all constituent elements in the original network to obtain $v_{\mathcal{I}}^{\rm DQ}$ would be computationally burdensome; instead, we utilize the linear approximation:

$$v_{\mathcal{I}}^{\rm DQ} \approx v_{\mathcal{I}}^{\star} + V_p P^{\star} + V_q Q^{\star}, \tag{18}$$

where $P^{\star} := [p_1^{\star}, \ldots, p_{|\mathcal{I}|}^{\star}]^{\rm T}$, $Q^{\star} := [q_1^{\star}, \ldots, q_{|\mathcal{I}|}^{\star}]^{\rm T}$, and $v_{\mathcal{I}}^{\star}$ is the linearization point. We pick $v_{\mathcal{I}}^{\star} = -Y_{\mathcal{I}\mathcal{I}}^{-1} Y_{g\mathcal{I}}^{\rm T} v_g^{\rm DQ}$, where $Y_{\mathcal{I}\mathcal{I}}$ and $Y_{g\mathcal{I}}$ are submatrices of the Kron-reduced admittance matrix (formally defined in (26)). The voltage $v_{\mathcal{I}}^{\star}$ is the *no-load voltage*, which is the voltage profile in the network with zero power injections at inverter buses [14]. With this choice,

$$V_p = \frac{v_{\rm base}}{3 s_{\rm base}} (\Gamma + j\Lambda), \quad V_q = \frac{v_{\rm base}}{3 s_{\rm base}} (\Lambda - j\Gamma), \tag{19}$$

where matrices Γ, Λ depend on the linearization point and network topology/constitution, and they are given by:

$$\begin{aligned} \Gamma &= R{\rm diag}\left(\frac{\cos\angle v_{\mathcal{I}}^{\star}}{|v_{\mathcal{I}}^{\star}|/v_{\rm base}}\right) - X{\rm diag}\left(\frac{\sin\angle v_{\mathcal{I}}^{\star}}{|v_{\mathcal{I}}^{\star}|/v_{\rm base}}\right), \\ \Lambda &= X{\rm diag}\left(\frac{\cos\angle v_{\mathcal{I}}^{\star}}{|v_{\mathcal{I}}^{\star}|/v_{\rm base}}\right) + R{\rm diag}\left(\frac{\sin\angle v_{\mathcal{I}}^{\star}}{|v_{\mathcal{I}}^{\star}|/v_{\rm base}}\right), \end{aligned} \tag{20}$$

with $R := y_{\rm base}\,{\rm Re}\{Y_{\mathcal{I}\mathcal{I}}^{-1}\}$, $X := y_{\rm base}\,{\rm Im}\{Y_{\mathcal{I}\mathcal{I}}^{-1}\}$, and $v_{\rm base} := |v_g^{\rm DQ}|$, $s_{\rm base}$ and $y_{\rm base}$ denoting the voltage, power and admittance base values. With the nominal virtual-bus voltages specified in (17), and the linear approximation of $v_{\mathcal{I}}^{\rm DQ}$ in (18), the virtual-transformers' turns ratios, $n \in \mathbb{C}^{|\mathcal{I}|}$ are:

$$n = {\rm diag}\left(\Phi\, \overline{v}_{\rm aux}^{\rm DQ}\right)^{-1} v_{\mathcal{I}}^{\rm DQ}, \tag{21}$$

which follows from the fact that $v_{\mathcal{I}}^{\rm DQ}$ are the voltages on the secondary side, and $\overline{v}_{\rm aux}^{\rm DQ}$ are the nominal voltages on the primary side of the transformers.

B. Dynamics of Virtual Network

The dynamics that characterize the virtual network are those of the aggregated-inverter models in the $|\mathcal{C}|$ clusters. These, coupled with pertinent algebraic equations that arise from the circuit laws that underlie the virtual network yield the real- and reactive-power grid injections. The dynamics of the aggregated inverters in the virtual network are:

$$\dot{x}^{\rm r} = A^{\rm r} x^{\rm r} + B^{\rm r} u_{\rm s}^{\rm r} + g^{\rm r}(x^{\rm r}, u_{\rm v}), \quad y^{\rm r} = \widehat{i}_{{\rm o}\mathcal{I}}^{\rm DQ}, \tag{22}$$

where $x^{\rm r} := [\widehat{x}_1^{\rm T}, \ldots, \widehat{x}_{|\mathcal{C}|}^{\rm T}]^{\rm T} \in \mathbb{R}^{15|\mathcal{C}|}$ collects the states corresponding to all the aggregated inverters in the reduced-order model (each $\widehat{x}_\ell \in \mathbb{R}^{15}$ has entries as shown in (7)). The power input $u_{\rm s}^{\rm r} = [u_{{\rm s},1}^{\rm T}, \ldots, u_{{\rm s},|\mathcal{C}|}^{\rm T}]^{\rm T} \in \mathbb{R}^{2|\mathcal{C}|}$, where (with slight abuse of notation) $u_{{\rm s},\ell} = \sum_{k \in \mathcal{I}_\ell} [p_k^{\star}, q_k^{\star}]^{\rm T}$, contains the power setpoints of the aggregated inverters; and the voltage input $u_{\rm v} = v_{\rm aux}^{\rm abc}$ (since the inverter terminal voltages are the virtual-bus voltages). The model output $y^{\rm r} = \widehat{i}_{{\rm o}\mathcal{I}}^{\rm DQ} \in \mathbb{C}^{|\mathcal{C}|}$ is the collection of the output currents of the aggregated inverters. Furthermore, $A^{\rm r} \in \mathbb{R}^{15|\mathcal{C}| \times 15|\mathcal{C}|}$, $B^{\rm r} \in \mathbb{R}^{15|\mathcal{C}| \times 2|{\rm C}|}$, $g^{\rm r} \in \mathbb{R}^{15|\mathcal{C}|} \times \mathbb{R}^{3 \times |\mathcal{C}|} \to \mathbb{R}^{15|\mathcal{C}|}$ are:

$$\begin{aligned} &A^{\rm r} = {\rm bdiag}(\widehat{A}_1, \ldots, \widehat{A}_{|\mathcal{C}|}),\ B^{\rm r} = {\rm bdiag}(\widehat{B}_1, \ldots, \widehat{B}_{|\mathcal{C}|}), \\ &g^{\rm r}(x^{\rm r}, u_{\rm v}) = \left[\widehat{g}_1(\widehat{x}_1, u_{{\rm v},1})^{\rm T}, \ldots, \widehat{g}_{|\mathcal{C}|}(\widehat{x}_{|\mathcal{C}|}, u_{{\rm v},|\mathcal{C}|})^{\rm T}\right]^{\rm T}, \end{aligned}$$

where $\widehat{A}_c$, $\widehat{B}_c$, and $\widehat{g}_c$ define the state-space model of the aggregated inverter for $|\mathcal{I}_c|$ parallel-connected inverters in the c-th cluster as in (6). To complete the model, we need to specify the terminal voltages of the inverters (which in this case are the voltages of the virtual buses $v_{\rm aux}^{\rm abc}$ (equivalently $v_{\rm aux}^{\rm DQ}$)), as well as the current injected into the grid for the new model. Kirchhoff's current law at the virtual buses is captured by $\widehat{i}_{{\rm o}\mathcal{I}}^{\rm DQ} = \Phi^{\rm T} i_{\rm aux}^{\rm DQ}$. Furthermore, the primary- and secondary-side quantities are related by:

$$\widehat{v}_{\mathcal{I}}^{\rm DQ} = {\rm diag}(n)\Phi\, v_{\rm aux}^{\rm DQ}, \quad \widehat{i}_{\mathcal{I}}^{\rm DQ} = {\rm diag}(n^{\rm H})^{-1} i_{\rm aux}^{\rm DQ}, \tag{23}$$

with the second equation arising from the conservation of power for an ideal transformer.

With the time-domain model of the network in place, we simplify the network dynamics by modeling them to be in steady-state. Writing (12) in phasor form, we get:

$$\widehat{i}_{\mathcal{E}}^{\rm DQ} = {\rm diag}(R_{\mathcal{E}} + j\omega_g L_{\mathcal{E}})^{-1} E^{\rm T} \widehat{v}^{\rm DQ}. \tag{24}$$

Let $\widehat{i}^{\rm DQ} \in \mathbb{C}^{|\mathcal{N}|+1}$ denote the vectors that collect the nodal current injections in DQ-frame, defined as follows:

$$\widehat{i}^{\rm DQ} = E\widehat{i}_{\mathcal{E}}^{\rm DQ} + j\omega_g {\rm diag}([0, C_{\mathcal{E}}^{\rm T}]^{\rm T})\widehat{v}^{\rm DQ}. \tag{25}$$

TABLE I: The z^{eff} value for the inverter buses.

Bus #	5	6	10	13	14	16	20	21	24	26	32	33	35	36	37
z^{eff}	0.031	0.031	0.047	0.055	0.055	0.055	0.080	0.080	0.080	0.088	0.16	0.16	0.14	0.14	0.080

TABLE II: Computation time in (s) to simulate the complete time-domain and aggregate models with different number of clusters.

	Time-domain	Aggregation (C-cluster)														
		$C=1$	2	3	4	5	6	7	8	9	10	11	12	13	14	15
Case #1	1035.4	1.71	2.56	3.53	3.78	3.93	4.23	4.45	4.82	4.85	4.87	4.88	4.89	4.91	4.93	4.94
Case #2	1031.5	1.76	2.45	3.54	3.82	3.95	4.27	4.46	4.81	4.83	4.86	4.87	4.90	4.93	4.95	4.96

Substituting for $\widehat{i}_{\mathcal{E}}^{\text{DQ}}$ from (24) in (25), we can write $\widehat{i}^{\text{DQ}} = Y\widehat{v}^{\text{DQ}}$, where Y is the network admittance matrix given in (10). Partition $\widehat{i}^{\text{DQ}} = [(\widehat{i}_{\mathcal{I}}^{\text{DQ}})^{\text{T}}, 0_{|\mathcal{Z}|}^{\text{T}}, -\widehat{i}_g^{\text{DQ}}]^{\text{T}}$ and $\widehat{v}^{\text{DQ}} = [(\widehat{v}_{\mathcal{I}}^{\text{DQ}})^{\text{T}}, \widehat{v}_{|\mathcal{Z}|}^{\text{T}}, v_g^{\text{DQ}}]^{\text{T}}$. Kron reduction of Y eliminates the zero-injection buses and yields:

$$\begin{bmatrix} \widehat{i}_{\mathcal{I}}^{\text{DQ}} \\ -\widehat{i}_g^{\text{DQ}} \end{bmatrix} = \begin{bmatrix} Y_{\mathcal{I}\mathcal{I}} & Y_{\mathcal{I}g} \\ Y_{\mathcal{I}g}^{\text{T}} & Y_{gg} \end{bmatrix} \begin{bmatrix} \widehat{v}_{\mathcal{I}}^{\text{DQ}} \\ v_g^{\text{DQ}} \end{bmatrix}. \tag{26}$$

Substituting $\widehat{v}_{\mathcal{I}}^{\text{DQ}}$ and $\widehat{i}_{\mathcal{I}}^{\text{DQ}}$ from (23) to (26), we have

$$\text{diag}(n^{\text{H}})^{-1} i_{\text{aux}}^{\text{DQ}} = Y_{\mathcal{I}\mathcal{I}}\,\text{diag}(n)\Phi v_{\text{aux}}^{\text{DQ}} + Y_{\mathcal{I}g} v_g^{\text{DQ}}, \tag{27}$$

$$-\widehat{i}_g^{\text{DQ}} = Y_{\mathcal{I}g}^{\text{T}}\,\text{diag}(n)\Phi v_{\text{aux}}^{\text{DQ}} + Y_{gg} v_g^{\text{DQ}}. \tag{28}$$

Then, we multiply both sides of (27) by $\Phi^{\text{T}}\text{diag}(n^{\text{H}})$ and use $\widehat{i}_{\text{o}\mathcal{I}}^{\text{DQ}} = \Phi^{\text{T}} i_{\text{aux}}^{\text{DQ}}$ to obtain:

$$v_{\text{aux}}^{\text{DQ}} = (\Pi^{\text{H}} Y_{\mathcal{I}\mathcal{I}} \Pi)^{-1} (\widehat{i}_{\text{o}}^{\text{DQ}} - \Pi^{\text{H}} Y_{\mathcal{I}g} v_g^{\text{DQ}}), \tag{29}$$

where $\Pi := \text{diag}(n)\Phi$. The dynamics of the system with the network represented in phasors and virtual buses introduced to aggregate inverters are given by (22) with $u_{\text{v}} = v_{\text{aux}}^{\text{abc}}$ obtained by applying Park's transformation to (29). From (28) and (29), we can write the grid current injection as a function of the output currents of the aggregate inverter model:

$$\widehat{i}_g^{\text{DQ}} = -Y_{\mathcal{I}g}^{\text{T}} \Pi \left(\Pi^{\text{H}} Y_{\mathcal{I}\mathcal{I}} \Pi\right)^{-1} (\widehat{i}_{\text{o}}^{\text{DQ}} - \Pi^{\text{H}} Y_{\mathcal{I}g} v_g^{\text{DQ}}) - Y_{gg} v_g^{\text{DQ}}, \tag{30}$$

following which, the real- and reactive-power injections into the grid bus g can be straightforwardly computed. The order of the reduced-order model dynamics with $|\mathcal{C}|$ clusters is $15|\mathcal{C}|$. Recall that the order of the original-network dynamics was $2(|\mathcal{E}|+|\mathcal{N}|)+15|\mathcal{I}|$. Since in practice we expect to have less clusters than the number of inverters, i.e., $|\mathcal{C}| << |\mathcal{I}|$, the reduced-order model is indeed computationally less burdensome. We demonstrate this, and the accuracy of the reduced-order model through simulations next.

V. Simulation Results

In this section, we validate the model-reduction method with numerical simulation results for a system of 15 inverters connected in a modified IEEE 37-bus network. The network is sketched in Fig. 4. The impedance of the lines connecting the buses in $\mathcal{Z}$ is $0.0081 + j0.00027\,\Omega$, except the lines: (17,18), (22,23), and (27,28); these have impedances that are 5 times that of the other lines. The impedance of the lines connecting the buses in $\mathcal{Z}$ to $\mathcal{I}$ is $0.0066 + j0.00010\,\Omega$. The shunt capacitors are identical, with capacitance of 1μF. The values of z^{eff} for the inverter buses are listed in Table I. All loads in the system are modeled as resistive loads with identical admittance of $0.05\,\Omega^{-1}$. The voltage and frequency of the grid are 288V and $2\pi \times 60$ rad/s, respectively. The power scaling parameters κ are selected to be uniformly distributed between 1 and 4. Parameters of the unscaled inverter (i.e., $\kappa = 1$) are obtained from [9]. The simulation is performed on a computer with an Intel Core i7-7700HQ processor @ 2.80GHz CPU and 8GB RAM.

We validate the accuracy of the reduced-order model through the following simulations: Case #1 Step change in $p^\star$ values from being uniformly distributed between 2-4kW to 4-5kW at $t = 1$s, and back to the original values at $t = 1.02$s. Case #2 Step change in $q^\star$ values from 0VAR to being uniformly distributed between 0-1kVAR at $t = 1$s, and back to 0VAR at $t = 1.02$s. For both cases, we stop the

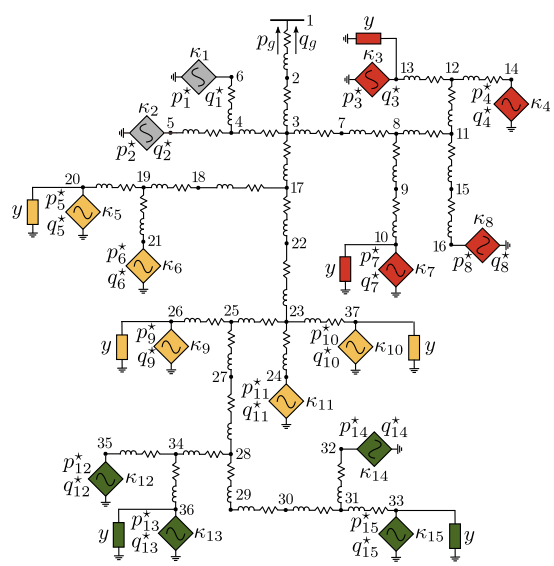

Fig. 4: IEEE 37-bus feeder system with 15 inverters and 7 loads. Notice that setpoints and ratings of the inverters are all different. Shaded colors represent clusters obtained by applying the electrical-distance clustering algorithm to the network with $C = 4$.

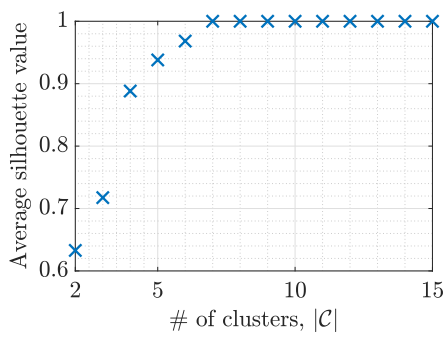

Fig. 5: The average silhouette value for different number of clusters.

TABLE III: Average error of the real and reactive power injection to the grid bus in (%) for one AC cycle after each step change in power setpoints.

		p_g		q_g	
		1st step	2nd step	1st step	2nd step
Case #1	1-cluster	1.58	4.71	0.47	8.4
	4-cluster	0.49	0.47	0.041	0.58
Case #2	1-cluster	0.25	0.24	0.62	9.32
	4-cluster	0.035	0.031	0.064	0.18

simulation at $t = 2$s. The running time of the simulations for the complete time-domain model and reduced-order models with 1 to 15 clusters are listed in Table II. Note that the 15-cluster model is the case when all inverter dynamics are retained, and the lines are modeled with phasors. As expected, it takes significantly longer to simulate the full time-domain model, and the reduced-order model with a single cluster has the least simulation time. Figure 5 shows the average silhouette value for different number of clusters. We choose 4 as the optimal number of clusters given its average silhouette value is above the reasonable threshold of 0.8. Figures 6 and 7 show the injected real and reactive power to the grid bus for case #1 and #2 of the following models: 1) the time-domain model and the 4-cluster and 15-cluster reduced-order models in Fig. 6, and 2) the parallel model (i.e., the case when the network is ignored so that all inverters are connected in parallel to the grid bus), the 1-cluster (i.e., without clustering) and 4-cluster reduced-order models in Fig. 7. The average errors for the 1-cluster and 4-cluster reduced-order models with respect to the 15-cluster reduced-order model for one AC cycle after each step change in the power setpoints are listed in Table III. The figures show that the reduced-order model with 4 clusters accurately captures the grid injections (indicating that accurate results can be obtained with modeling few clusters) and it has better transient performance than the 1-cluster reduced-order model while the model where the inverters are simply assumed to be in parallel (by neglecting the distribution network) is associated with errors in steady state and through the transients because the power losses and damping induced by the network are neglected.

Furthermore, we perform simulations with different sets of line impedances for the IEEE 37-bus system. In particular, we consider line impedances with r/x ratios of 0.1, 1, and 5. In these simulations, all inverters have the same power scaling parameters κ as 1, and the same power setpoints with p^* values having step changes from 3kW to 4kW at $t = 1s$ and back to the original values at $t = 1.02$s, and $q^* = 0$VAR. The real power injection to the grid bus for the 1-cluster, 4-cluster, and 15-cluster reduced-order models are shown in Fig. 8. The figures show that the 4-cluster model performs well regardless of the r/x ratio of the line impedances, while the performance of the 1-cluster model degrades as the r/x ratio increases (i.e., the network becomes more resistive).

VI. Concluding Remarks and Future Work

We presented a model-reduction method for networks of inverters with different power ratings and reference-power setpoints, connected to an arbitrary network topology. This method involves: i) clustering the inverters based on their electrical distance from the grid, ii) transferring the inverters in each group to their respective virtual buses with the aid of ideal transformers and linear approximation of the power-flow equations, and iii) aggregating the inverters in each of the buses to an equivalent inverter using our previous work on the aggregate model for parallel-connected grid-tied three-phase inverters. Numerical simulations established the accuracy and computational benefits of the approach. Future work involves leveraging these models to examine dynamic interactions in mixed-machine-inverter systems. Accommodating different load models, in particular, constant-power loads, in the aggregation approach is another important direction for future work.

References

[1] M. Rasheduzzaman, J. A. Mueller, and J. W. Kimball, "An accurate small-signal model of inverter- dominated islanded microgrids using *dq* reference frame," *IEEE Trans. Emerg. Sel. Topics Power Electron.*, vol. 2, pp. 1070–1080, Dec 2014.

[2] J. A. Mueller, M. Rasheduzzaman, and J. W. Kimball, "A model modification process for grid-connected inverters used in islanded microgrids," *IEEE Trans. Energy Convers.*, vol. 31, pp. 240–250, Mar 2016.

[3] M. Prodanovic and T. C. Green, "Control and filter design of three-phase inverters for high power quality grid connection," *IEEE Trans. Power Electron.*, vol. 18, pp. 373–380, Jan 2003.

[4] E. Twining and D. G. Holmes, "Grid current regulation of a three-phase voltage source inverter with an LCL input filter," *IEEE Trans. Power Electron.*, vol. 18, pp. 888–895, May 2003.

[5] N. Pogaku, M. Prodanovic, and T. C. Green, "Modeling, analysis and testing of autonomous operation of an inverter-based microgrid," *IEEE Trans. Power Electron.*, vol. 22, pp. 613–625, Mar 2007.

[6] C. A. Plet, M. Graovac, T. C. Green, and R. Iravani, "Fault response of grid-connected inverter dominated networks," in *IEEE PES General Meeting*, pp. 1–8, Jul 2010.

[7] V. Purba, S. V. Dhople, S. Jafarpour, F. Bullo, and B. B. Johnson, "Reduced-order structure-preserving model for parallel-connected three-phase grid-tied inverters," in *IEEE 18th Workshop on Control and Modeling for Power Electronics*, pp. 1–7, Jul 2017.

[8] V. Purba, B. B. Johnson, M. Rodriguez, S. Jafarpour, F. Bullo, and S. V. Dhople, "Reduced-order aggregate model for parallel-connected single-phase inverters," *IEEE Trans. Energy Convers.*, vol. 34, pp. 824–837, Jun 2019.

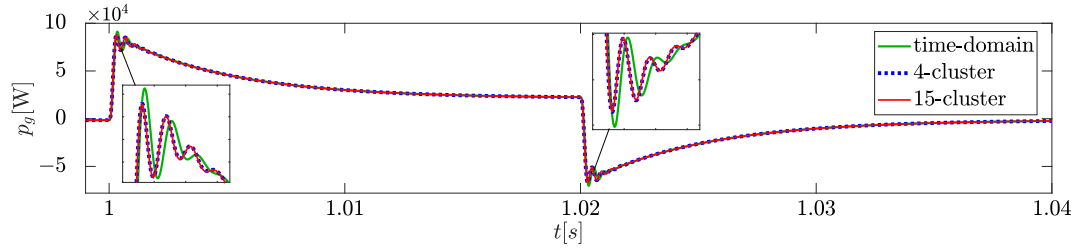

(a) Real power injection to the grid bus

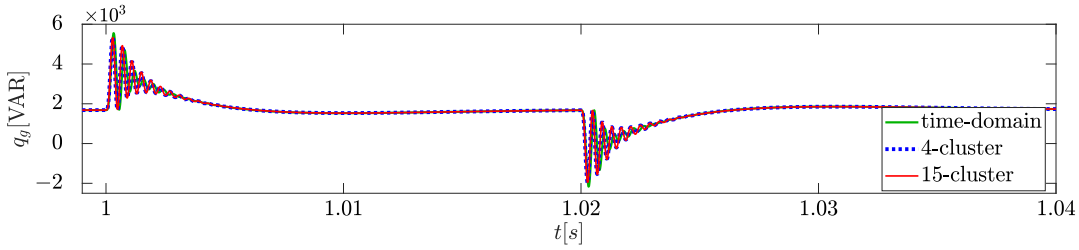

(b) Reactive power injection to the grid bus

Fig. 6: Simulation results for Case #1: Real-power setpoints $p^\star$ are selected from a uniform distribution between 2-4kW for $t < 1$s, 4-5kW for $1 \leq t < 1.02$s, and back to the original setpoints for $t \geq 1.02$s. Reactive-power setpoints $q^\star$ are 0VAR for $t \geq 0$s.

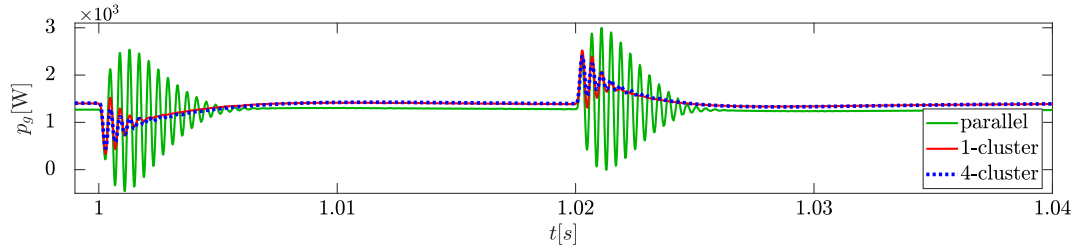

(a) Real power injection to the grid bus

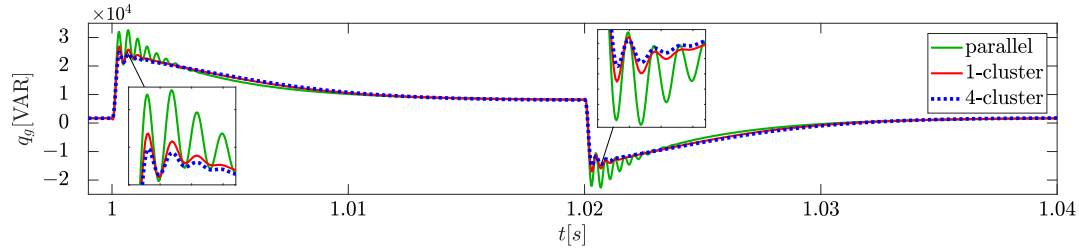

(b) Reactive power injection to the grid bus

Fig. 7: Simulation results for Case #2: Real-power setpoints $p^\star$ are selected from uniform distribution between 2-4kW for $t \geq 0$s. Reactive-power setpoints $q^\star$ are 0VAR for $t < 1$s, uniformly distributed between 0-1kVAR for $1 \leq t < 1.02$s, and 0VAR for $t \geq 1.02$s.

[9] V. Purba, S. V. Dhople, S. Jafarpour, F. Bullo, and B. B. Johnson, "Network-cognizant model reduction of grid-tied three-phase inverters," in *Allerton Conference on Communication, Control, and Computing*, pp. 157–164, Oct 2017.

[10] Z. Shuai, Y. Peng, X. Liu, Z. Li, J. M. Guerrero, and Z. J. Shen, "Dynamic equivalent modeling for multi-microgrid based on structure preservation method," *IEEE Trans. Smart Grid*, vol. 10, pp. 3929–3942, Jul 2019.

[11] A. J. Germond and R. Podmore, "Dynamic aggregation of generating unit models," *IEEE Trans. Power App. Syst*, vol. PAS-97, pp. 1060–1069, Jul 1978.

[12] M. L. Ourari, L. A. Dessaint, and V.-Q. Do, "Dynamic equivalent modeling of large power systems using structure preservation technique," *IEEE Trans. Power Syst.*, vol. 21, pp. 1284–1295, Aug 2006.

[13] J. H. Chow, *Power System Coherency and Model Reduction*. Springer, 2013.

[14] S. V. Dhople, S. S. Guggilam, and Y. C. Chen, "Linear approximations to AC power flow in rectangular coordinates," in *Allerton Conference on Communication, Control, and Computing*, pp. 211–217, Sep 2015.

[15] S. Bolognani and F. Dörfler, "Fast power system analysis via implicit linearization of the power flow manifold," in *Allerton Conference on Communication, Control, and Computing*, pp. 402–409, Sep 2015.

[16] S. Bolognani and S. Zampieri, "On the existence and linear approximation of the power flow solution in power distribution networks," *IEEE Trans. Power Syst.*, vol. 31, pp. 163–172, Jan 2016.

[17] L. Ding, Z. Ma, P. Wall, and V. Terzija, "Graph spectra based controlled islanding for low inertia power systems," *IEEE Trans. Power Del.*, vol. 32, pp. 302–309, Feb 2017.

[18] E. Cotilla-Sanchez, P. D. H. Hines, C. Barrows, S. Blumsack, and M. Patel, "Multi-attribute partitioning of power networks based on

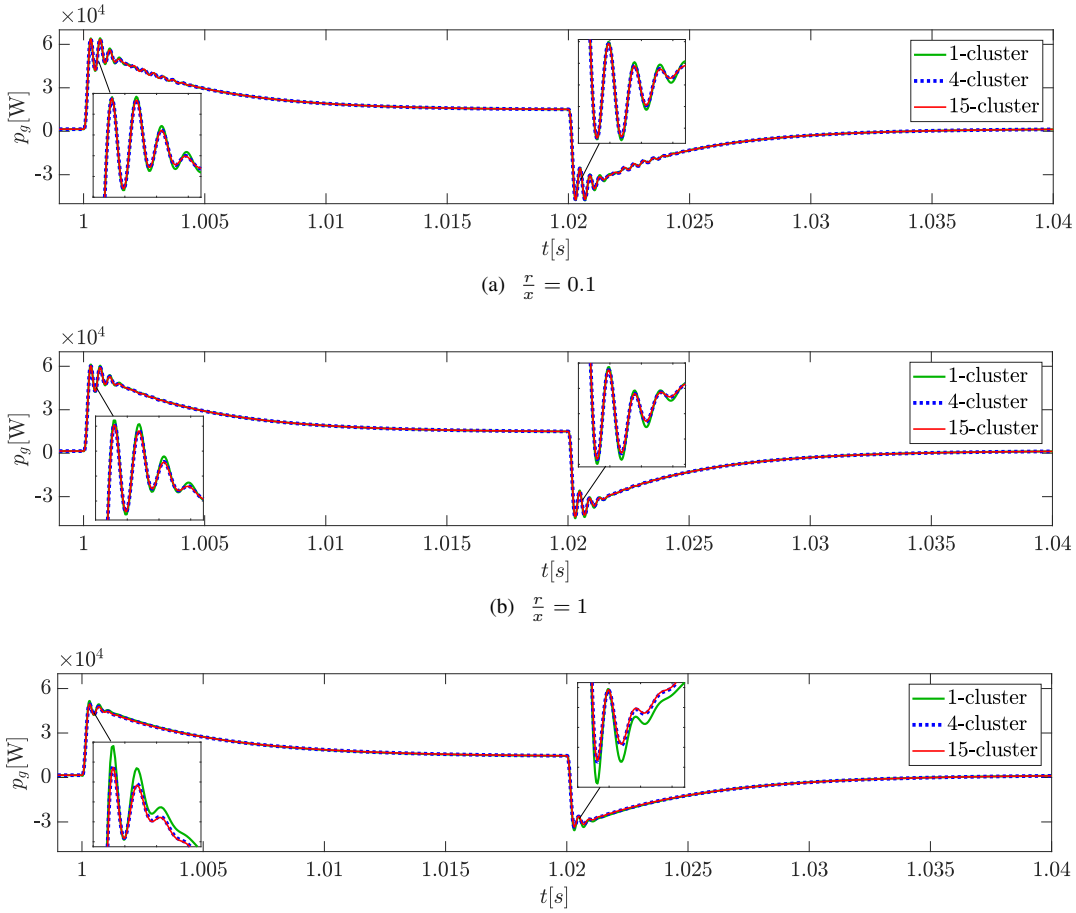

(a) $\frac{r}{x} = 0.1$

(b) $\frac{r}{x} = 1$

(c) $\frac{r}{x} = 5$

Fig. 8: Real power injection to the grid bus for various r/x ratio values.

electrical distance," *IEEE Trans. Power Syst.*, vol. 28, pp. 4979–4987, Nov 2013.

[19] R. J. Sánchez-García, M. Fennelly, S. Norris, N. Wright, G. Niblo, J. Brodzki, and J. W. Bialek, "Hierarchical spectral clustering of power grids," *IEEE Trans. Power Syst.*, vol. 29, pp. 2229–2237, Sep 2014.

[20] A. Ishchenko, J. M. A. Myrzik, and W. L. Kling, "Dynamic equivalencing of distribution networks with dispersed generation using Hankel norm approximation," *IET Generation, Transmission Distribution*, vol. 1, pp. 818–825, Sep 2007.

[21] F. O. Resende, J. Matevosyan, and J. V. Milanovic, "Application of dynamic equivalence techniques to derive aggregated models of active distribution network cells and microgrids," in *2013 IEEE Grenoble Conference*, pp. 1–6, Jun 2013.

[22] A. K. Jain and R. C. Dubes, *Algorithms for Clustering Data*. Upper Saddle River, NJ, USA: Prentice-Hall, Inc., 1988.

[23] K. Wagstaff, C. Cardie, S. Rogers, and S. Schrödl, "Constrained K-means clustering with background knowledge," in *Proceedings of the 18th International Conference on Machine Learning*, (San Francisco, CA, USA), pp. 577–584, Morgan Kaufmann Publishers, 2001.

[24] R. Xu and D. Wunsch, "Survey of clustering algorithms," *IEEE Trans. Neural Netw.*, vol. 16, pp. 645–678, May 2005.

[25] G. W. Milligan and M. C. Cooper, "An examination of procedures for determining the number of clusters in a data set," *Psychometrika*, vol. 50, pp. 159–179, Jun 1985.

[26] R. Tibshirani, G. Walther, and T. Hastie, "Estimating the number of clusters in a data set via the gap statistic," *Journal of the Royal Statistical Society: Series B (Statistical Methodology)*, vol. 63, no. 2, pp. 411–423, 2001.

[27] C. A. Sugar and G. M. James, "Finding the number of clusters in a dataset: An information-theoretic approach," *Journal of the American Statistical Association*, vol. 98, no. 463, pp. 750–763, 2003.

[28] P. J. Rousseeuw, "Silhouettes: A graphical aid to the interpretation and validation of cluster analysis," *Journal of Computational and Applied Mathematics*, vol. 20, pp. 53–65, 1987.

[29] L. Kaufman and P. J. Rousseeuw, *Finding Groups in Data: An Introduction to Cluster Analysis*. John Wiley & Sons, 1990.

[30] A. P. Reynolds, G. Richards, B. de la Iglesia, and V. J. Rayward-Smith, "Clustering rules: A comparison of partitioning and hierarchical clustering algorithms," *Journal of Mathematical Modelling and Algorithms*, vol. 5, pp. 475–504, Dec 2006.

[31] L. Luo and S. V. Dhople, "Spatiotemporal model reduction of inverter-based islanded microgrids," *IEEE Trans. Energy Convers.*, vol. 29, pp. 823–832, Dec 2014.

[32] M. Rasheduzzaman, J. A. Mueller, and J. W. Kimball, "Reduced-order small-signal model of microgrid systems," *IEEE Trans. Sustain. Energy*, vol. 6, pp. 1292–1305, Oct 2015.

[33] O. O. Ajala, A. D. Domínguez-García, and P. W. Sauer, "A hierarchy of models for inverter-based microgrids," in *Energy Markets and Responsive Grids: Modeling, Control and Optimization* (S. Meyn, T. Samad, S. Glavaski, I. Hiskens, and J. Stoustrup, eds.), Berlin: Springer-Verlag, 2017.

[34] P. J. Hart, R. H. Lasseter, and T. M. Jahns, "Enforcing coherency in droop-controlled inverter networks through use of advanced voltage regulation and virtual impedance," in *IEEE Energy Conversion Congress and Exposition*, pp. 3367–3374, Oct 2017.

[35] C. Li, J. Xu, and C. Zhao, "A coherency-based equivalence method for mmc inverters using virtual synchronous generator control," *IEEE Trans. Power Del.*, vol. 31, pp. 1369–1378, Jun 2016.

[36] P. J. Hart, R. H. Lasseter, and T. M. Jahns, "Reduced-order harmonic

modeling and analysis of droop-controlled distributed generation networks," in *IEEE 7th International Symposium on Power Electronics for Distributed Generation Systems (PEDG)*, pp. 1–9, Jun 2016.

[37] M. M. S. Khan, Y. Lin, B. Johnson, V. Purba, M. Sinha, and S. Dhople, "A reduced-order aggregated model for parallel inverter systems with virtual oscillator control," in *2018 IEEE 19th Workshop on Control and Modeling for Power Electronics (COMPEL)*, pp. 1–6, Jun 2018.

[38] P. Kundur, N. J. Balu, and M. G. Lauby, *Power system stability and control*, vol. 7. McGraw-hill New York, 1994.

[39] F. Dörfler and F. Bullo, "Kron reduction of graphs with applications to electrical networks," *IEEE Trans. Circuits Syst. I, Reg. Papers*, vol. 60, pp. 150–163, Jan 2013.

Victor Purba (S'15) received the Bachelor's and M.S. degrees in electrical engineering in 2014 and 2016, respectively, from University of Minnesota, Minneapolis, MN, USA, where he is currently pursuing the Ph.D. degree in electrical engineering. His research interests include modeling, analysis, and control of power systems with the integration of renewable energy sources.

Brian Johnson (S'08, M'13) obtained the M.S. and Ph.D. degrees in electrical and computer engineering from the University of Illinois at Urbana-Champaign, Urbana, in 2010 and 2013, respectively. He is an Assistant Professor within the Department of Electrical Engineering at the University of Washington. Prior to joining the faculty at the University of Washington in 2018, he was an Electrical Engineer with the National Renewable Energy Laboratory in Golden, CO. He was awarded a National Science Foundation Graduate Research Fellowship in 2010, and currently serves as an Associate Editor for the IEEE Transactions on Energy Conversion. His research interests are in renewable energy systems, power electronics, and control systems.

Saber Jafarpour (M'16) is a Postdoctoral research fellow with the Center for Control, Dynamical Systems and Computation at the University of California, Santa Barbara. He received his Ph.D. in 2016 from the Department of Mathematics and Statistics at Queen's University. His research interests include analysis of network systems with application to power grids and geometric control theory.

Francesco Bullo (S'95, M'99, SM'03, F'10) is a Professor with the Mechanical Engineering Department and the Center for Control, Dynamical Systems and Computation at the University of California, Santa Barbara. He was previously associated with the University of Padova (Laurea degree in Electrical Engineering, 1994), the California Institute of Technology (Ph.D. degree in Control and Dynamical Systems, 1999), and the University of Illinois. His research interests focus on network systems and distributed control with application to robotic coordination, power grids and social networks. He is the coauthor of "Geometric Control of Mechanical Systems" (Springer, 2004) and "Distributed Control of Robotic Networks" (Princeton, 2009); his "Lectures on Network Systems" (CreateSpace, 2018) is available on his website. He is a Fellow of IEEE and IFAC. He has served on the editorial boards of IEEE, SIAM, and ESAIM journals, and served as 2018 IEEE CSS President.

Sairaj V. Dhople (M'13) received the B.S., M.S., and Ph.D. degrees in electrical engineering from the University of Illinois at Urbana-Champaign, Urbana, IL, USA, in 2007, 2009, and 2012, respectively. He is currently an Associate Professor with the Department of Electrical and Computer Engineering, University of Minnesota, Minneapolis, MN, USA. His research interests include modeling, analysis, and control of power electronics and power systems with a focus on renewable integration. Dr. Dhople received the National Science Foundation CAREER Award in 2015 and the Outstanding Young Engineer Award from the IEEE Power and Energy Society in 2019. He is an Associate Editor for the IEEE Transactions on Energy Conversion and the IEEE Transactions on Power Systems.